Functionalizing Nanocrystalline Metal Oxide Electrodes With Robust Synthetic Redox Proteins

Emmanuel Topoglidis,[a] Bohdana M. Discher,[b] Christopher C. Moser,[b] P. Leslie Dutton,[b] and James R. Durrant*[a]

De novo designed synthetic redox proteins (maquettes) are structurally simpler, working counterparts of natural redox proteins. The robustness and adaptability of the maquette protein scaffold are ideal for functionalizing electrodes. A positive amino acid patch has been designed into a maquette surface for strong electrostatic anchoring to the negatively charged surfaces of nanocrystalline, mesoporous TiO_2 and SnO_2 films. Such mesoporous metal oxide electrodes offer a major advantage over conventional planar gold electrodes by facilitating formation of high optical density, spectroelectrochemically active thin films with protein loading orders of magnitude greater (up to 8 nmol cm^{-2}) than that achieved with gold electrodes. The films are stable for weeks, essentially all immobilized-protein display rapid, reversible electrochemistry. Furthermore, carbon monoxide ligand binding to the reduced heme group of the protein is maintained, can be sensed optically and reversed electrochemically. Pulsed UV excitation of the metal oxide results in microsecond or faster photoreduction of an immobilized cytochrome and millisecond reoxidation. Upon substitution of the heme-group Fe by Zn, the light-activated maquette injects electrons from the singlet excited state of the Zn protoporphyrin IX into the metal oxide conduction band. The kinetics of cytochrome/metal oxide interfacial electron transfer obtained from the electrochemical and photochemical data obtained are discussed in terms of the free energies of the observed reactions and the electronic coupling between the protein heme group and the metal oxide surface.

Introduction

De novo design of synthetic redox proteins (maquettes) generates a novel class of macromolecules that minimize the structural complexity of natural proteins whilst retaining the desired functional properties in an adaptable and robust amino acid scaffold.[1–2] Redox protein maquettes serve as test beds for studying biological electron transfer.[3] They have been employed to identify the requirements for protein assembly and incorporation of redox cofactors, and to determine the factors controlling in situ electron transfer and electrochemistry. Furthermore, maquettes are designed to be environmentally robust to foster the development of biochemical devices for technological applications ranging from driving catalytic redox reactions to biosensors and bioremediation. By adapting the pattern of amino acid charges on the maquette surface, the interaction with electrode surfaces and therefore the electron transfer to/from the maquettes can be readily controlled.[4] However, previous surface electrochemical studies of protein maquettes have been constrained to planar electrodes[4, 5] and the monolayer surface densities of self-adsorbed maquettes provide only small, milliOD (OD, optical density units) spectroscopic signals. This major obstacle can be surmounted with recent advances in metal oxide electrodes.

Nanocrystalline, mesoporous metal oxide electrodes combine the properties of high surface area, optical transparency, and electrical semiconductivity with excellent stability and ease of fabrication. They are thus attracting attention for an increasingly wide range of both scientific studies and technological device applications. Many of these applications involve increasing the functionality of such films by the adsorption of molecular or biomolecular species to the surface of their constituent metal oxide nanoparticles. This approach has been used, for example, in the development of dye-sensitized photovoltaic cells, where molecular dyes are employed to sensitize the films to visible light,[6] and in the development of electrochromic displays, where the application of an electrical bias is employed to modulate the redox state, and therefore the color of redox molecules immobilized on the film surface.[7] The approach has been further extended to the immobilization of a range of biomolecules, including redox proteins, enzymes, and nucleic acids, which leads to a range of bioelectrochemical and biosensing functions.[8–12]

[a] *Dr. J. R. Durrant, Dr. E. Topoglidis*
Center of Electronic Materials and Devices
Department of Chemistry
Imperial College, South Kensington, London SW7 2AZ (UK)
Fax: (+44) 20-75945801
E-mail: j.durrant@ic.ac.uk

[b] *Dr. B. M. Discher, Prof. C. C. Moser, Prof. P. L. Dutton*
Johnson Research Foundation
Department of Biochemistry and Biophysics
University of Pennsylvania, Philadelphia 19104 (USA)

  DOI: 10.1002/cbic.200300707

We have combined progress in maquette design with that in the development of metal oxide electrodes to immobilize a synthetic redox protein maquette on nanocrystalline TiO_2 and SnO_2 electrodes. Herein, we demonstrate that protein maquettes can indeed be readily and stably immobilized upon such electrodes. By means of electrochemical, spectroelectrochemical, and photochemical studies, we have investigated the details of maquette function and interaction with the electrode surface. The protein maquette selected for this study, a four-α-helix bundle, binds a heme moiety (iron protoporphyrin IX) analogous to native cytochrome *b*, and exhibits reversible electrochemistry and specific ligatation of CO when bound to modified gold electrodes.[4] Nanocrystalline electrodes not only provide high optical density spectral changes confirming these functions but also the means for convenient rapid photoinduced electron transfer from electrode to maquette. In addition, by exchanging the Fe species in the heme group for Zn protoporphyrin, we enable the complementary photoinduced electron transfer from light-activated maquette to electrode.

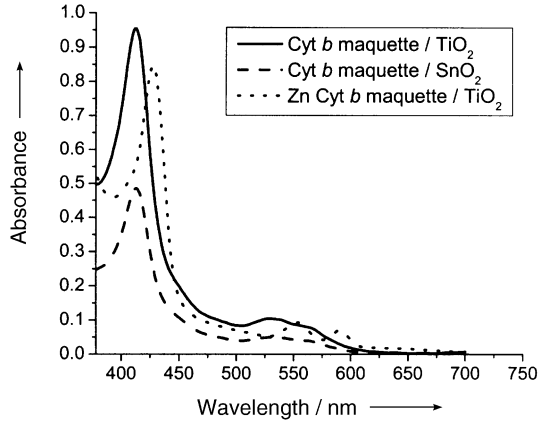

Figure 1. *Absorption spectra of a 4-μm-thick nanoporous SnO_2 and an 8-μm-thick nanoporous TiO_2 film after the immobilization of the Fe cyt* b *maquette on their surfaces. The spectrum of an 8-μm-thick nanoporous TiO_2 film after the immobilization of Zn cyt* b *maquette is also shown. All spectra shown are those obtained after subtraction of the spectra recorded for protein-free films.*

Results

Protein immobilization

Immobilization of native redox proteins such as cytochrome *c* (cyt *c*) and hemoglobin from aqueous solutions on nanocrystalline metal oxide films may be readily achieved at 4 °C with a high binding stability and no detectable denaturation.[8–10] The mesoporous structure of such films greatly enhances the active surface available for protein binding compared to the geometrical area (by a factor of up to 850 for an 8-μm-thick TiO_2 film). The binding appears to be largely electrostatic and is strongly influenced by the pH value and ionic strength of the solution, and by the protein and film charges.[9]

At the pH value of the solution employed in this study (pH 7.0), both the TiO_2 and SnO_2 films are expected to have negative surface charges (zero charge at pH 5.5 and 5, respectively), which favors electrostatic interactions with the cluster of positively charged lysine residues located on the heme-binding end of the cyt *b* maquette. Strong binding was indeed observed for both the Fe and Zn cyt *b* maquettes and resulted in orange and yellow coloration of the metal oxide films, respectively. Immobilization was quantified by UV/Visible absorption spectroscopy, as illustrated in Figure 1, which shows spectra obtained following immobilization on 8-μm-thick TiO_2 and 4-μm-thick SnO_2 films. The absorption spectra of the immobilized iron(III) cyt *b* maquette show the characteristic heme absorption bands at 412, 531, and 560 nm on both electrode surfaces. The absorption spectrum of the immobilized Zn cyt *b* maquette shows bands at 427, 554, and 591 nm. All these bands are in good agreement with the solution spectra of iron(III) cyt *b* and Zn cyt *b*, respectively, which suggests the absence of protein denaturation.[8–10] Indeed, the excellent stability of immobilized maquettes throughout the course of our experiments (2 – 3 weeks) is consistent with our previous observation that the stability of immobilized proteins is greater than that of the same proteins suspended in solution.[9] This excellent stability probably derives from the hydrophilic nature of the metal oxide surface and/or spatial restrictions on the conformational changes of the immobilized maquettes.

For both the Fe and Zn porphyrin maquette films, the achieved protein loading approaches a monolayer coverage over the internal surface of the porous films. The protein loadings of the iron(III) cyt *b* maquette/metal oxide films were determined from the observed optical densities. By using an extinction coefficient of $120\,000\ M^{-1}cm^{-1}$ at 412 nm for the iron(III) cyt *b* maquette, loadings of 8 and 3 nmol were calculated for the 8-μm TiO_2 and 4-μm SnO_2 films, respectively (film geometric areas of 1 cm^2). Film surface areas of 800 and 300 cm^2 were determined from previous Brunauer, Emmett, and Teller (BET) gas adsorption analyses for the TiO_2 and SnO_2 films, respectively; these coverages both correspond to approximately 1700 $Å^2$ molecule^{-1}. Comparable coverage was achieved previously on gold electrodes coated with a monolayer of 11-mercaptoudecanoic acid (2300 $Å^2$ molecule^{-1}).[4]

Cyclic voltammetry

The nanoporous SnO_2 electrode exhibits a greater electrical conductivity than the TiO_2 electrode over the potential range of interest, as we have reported elsewhere.[13] Our cyclic voltammetry (CV) studies therefore focused on Fe cyt *b* maquette/SnO_2 films. Experiments were carried out in degassed, protein-free buffer solution, without the use of any electron transfer promoters or mediators. Typical CV data are shown in Figure 2 for both the protein-loaded film and for the protein-free control film (inset). The data for the control, protein-free film show the characteristic charging/decharging currents assigned to electron injection into conduction band/sub-band-gap states of the SnO_2 film. The voltammogram integrates to approximately zero, which indicates that faradaic currents are negligible. It is further apparent that the SnO_2 film exhibits significant charging, and therefore conductivity, for potentials of up to 0.2 V versus Ag/AgCl. Data for the protein-loaded film are shown as a function of

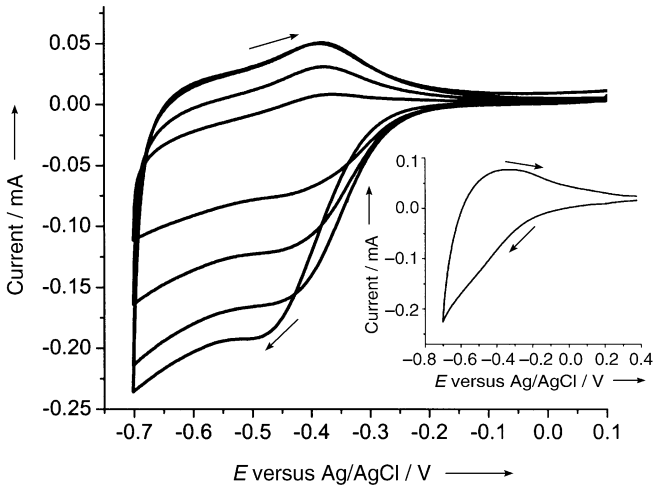

Figure 2. *Cyclic voltamograms of Fe cyt* b *maquette immobilized on a nanoporous SnO_2 electrode in phosphate buffer (0.01 M, pH 7.0) at 25, 50, 75, and 100 mV s^{-1} (from lowest to highest peak currents). The CV at 0.1 V s^{-1} in the same buffer for a protein-free nanoporous SnO_2 film is also shown (inset).*

scan rate. These voltammograms show clearly defined oxidation and reduction peaks superimposed on the film charging/decharging currents. These peaks are assigned to maquette reduction/oxidation, an assignment that is confirmed by spectroelectrochemical data detailed below. Peak positions and currents are plotted as a function of scan rate in Figure 3.

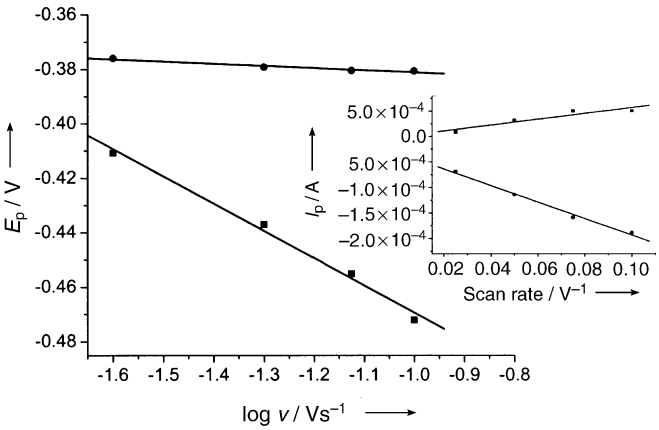

Figure 3. *Plots of cathodic (●) and anodic (■) peak potentials versus the logarithm of the scan rate,* v. *The inset shows plots of the cathodic (●) and anodic (■) peak currents versus scan rate.*

Analogous data collected for Fe cyt *b* maquette/TiO_2 films yielded very similar reduction peaks to those of the SnO_2 films; however, as a result of the more limited conductivity of the TiO_2 films, the oxidation peak could only be observed at the slowest scan rate (data not shown). From the data on the SnO_2 electrode we obtain a midpoint potential for the immobilized Fe cyt *b* maquette of -0.39 V versus Ag/AgCl, similar to the value of -0.43 V we reported previously for planar gold electrodes coated with 11-mercaptoundecanoic acid.[12]

Integration of the oxidation/reduction peak areas indicates loadings of electroactive Fe cyt *b* maquette of around 2.2 nmol cm^{-2} film. This loading is of a similar magnitude to that obtained from the optical absorption spectra and indicates that a high proportion of the immobilized protein is electroactive, which is consistent with spectrochemical data detailed below. This high activity is indicative of a strong binding and favorable orientation of the cyt *b* maquette on the electrode surface. This conclusion is further supported by our observation that the CV response showed excellent stability with no detectable perturbation after the 5 – 10 repeat scans typically carried out.

The scan-rate dependence of the reduction and oxidation potentials shown in Figure 3 for the Fe cyt *b* maquette/SnO_2 films exhibits a clear asymmetry. The reduction peak shows a clear dependence upon scan rate typical of interfacial electron-transfer-limited reduction. By using the Laviron analysis,[14] we obtain a charge transfer coefficient (α) of 0.6 and an electron transfer rate constant (k_s) for this reduction reaction at zero overpotential of 1.5 ± 0.3 s^{-1}. The oxidation peak potential was observed to be scan-rate independent up to the highest scan rate employed (0.1 V s^{-1}). The use of higher scan rates resulted in loss of a well-defined oxidation peak, attributed to electrical conductivity limitations of the SnO_2 film. The absence of any scan-rate dependence is indicative of an electron transfer rate constant for this oxidation reaction of more than 100 s^{-1}.

Spectroelectrochemistry

The assignment of the CV peaks to cyt *b* maquette reduction and oxidation was confirmed spectroelectrochemically by placing the working electrode of the spectroelectrochemical cell employed for the CV studies in the sample beam of the UV/Vis spectrometer. Figure 4 shows typical spectroelectrochemical data for the Fe cyt *b* maquette/SnO_2 films. Spectra are shown as a function of applied potentials in the range -0.1 to -0.5 V versus Ag/AgCl. The application of a negative potential results in a shift in the Soret band peak from 412 to 426 nm and an increase in the intensity of the sharp α and β bands at 527 and

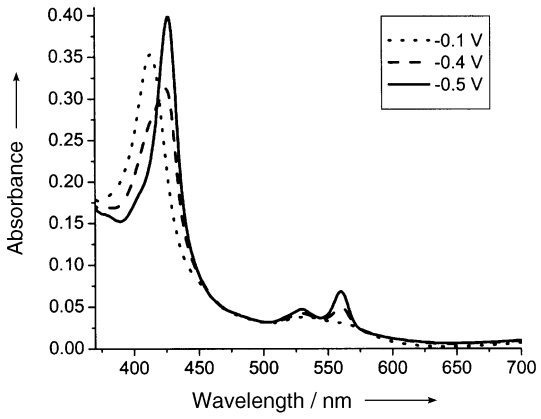

Figure 4. *UV/Vis absorption spectra for electrochemical reduction of the oxidized iron(III) cyt* b *maquette immobilized on a nanoporous SnO_2 film at increasingly negative potentials (-0.1 to -0.5 V).*

560 nm. These spectral changes are in accordance with solution spectra for the reduction of the cyt *b* maquette from its Fe^{III} to its Fe^{II} state,[15] and are indicative of essentially complete (> 90%) reduction of the immobilized cyt *b* maquette. Reoxidation of the immobilized Fe cyt *b* maquette on the nanoporous SnO_2 electrodes could be achieved by applying a positive bias (0 – 0.2 V) to the SnO_2 electrode (data not shown).

Figure 5 shows the absorbance of the reduced Fe cyt *b* maquette on the SnO_2 film as a function of the applied negative potential, as determined from the spectroelectrochemical data shown in Figure 4, and a fit of these data to the Nernst equation. A good fit is obtained to the Nernst equation, which yields a midpoint potential of -0.4 ± 0.01 V versus Ag/AgCl, a result in good agreement with the CV data and our previous studies on gold electrodes.[4]

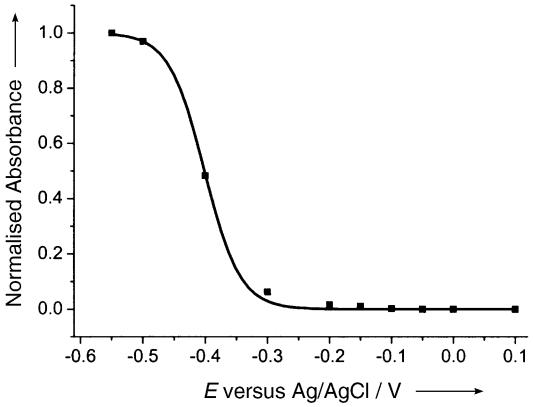

Figure 5. *The proportion of Fe cyt* b *maquette reduced on a nanoporous SnO_2 film can be determined from its optical absorbance at 560 nm as a function of the applied potential.*

CO binding

Figure 6 shows the absorption spectra for the Fe cyt *b* maquette/SnO_2 film both in the presence and absence of carbon monoxide. The absorption spectrum of the oxidized maquette was found to be independent of the presence of CO, which indicates[15] a low CO binding constant to the oxidized heme, as expected. After electrochemical reduction of the immobilized cyt *b* maquette to the iron(II) state by the application of -0.5 V, clear spectral changes indicative of CO ligation were observed. The shift in the heme Soret absorption maximum from 426 to 419 nm accompanied by the appearance of α and β absorption bands at 537 and 565 nm is in good agreement with solution phase studies of CO binding.[15] Such CO binding has previously been attributed to CO ligation to the ferrous bis-histidyl heme groups in the maquette by displacement of one of the histidine residues. CO binding was fully reversible, with the application of a positive ($+0.2$ V) potential resulting in heme oxidation, concomitant CO release, and return of the heme group to its bis-histidyl ligation state. These observations provide further confirmation of the structural and functional integrity of the immobilized maquette.

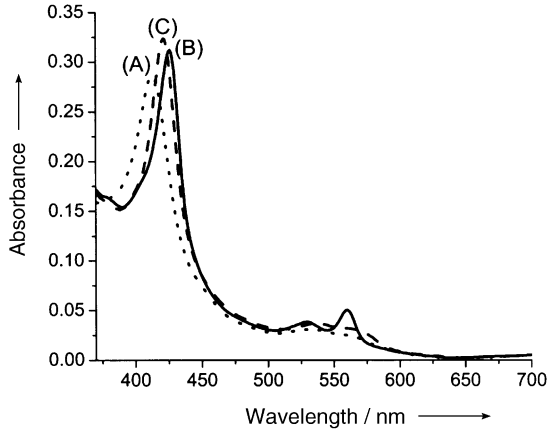

Figure 6. *Absorption spectra of (A) iron(III) cyt* b *maquette, (B) iron(II) cyt* b *maquette, and (C) carbonyl iron(II) cyt* b *maquette immobilized on a nanoporous SnO_2 film. Iron(II) cyt* b *was generated by the application of -0.5 V electrochemically. Carbonyl iron(II) cyt* b *maquette was subsequently generated by the addition of 3 μM CO to the electrolyte.*

Transient spectroscopy of protein/electrode electron transfer

The optical transparency and high surface area of the metal oxide films allow electrochemical studies of interfacial electron transfer processes to be complemented by transient optical techniques. Two methodologies have been reported that employ transient optical spectroscopies to interrogate electron transfer dynamics between the natural Fe-mesoporphyrin-containing cyt *c* and TiO_2 electrodes. After pulsed band-gap excitation of TiO_2 electrodes, either photoreduction of adsorbed iron(III) cyt *c* or photooxidation of adsorbed iron(II) cyt *c* was observed depending on the redox state of the adsorbed cytochrome prior to the pulsed excitation.[8] No electron transfer was observed following direct excitation of the Fe cyt *c*; this observation was attributed to the short lifetime of the Fe heme excited state. However, with zinc-substituted cyt *c*, efficient charge separation was observed following photoexcitation of the Zn cyt *c*, monitored both by quenching of the singlet excited state lifetime of the Zn cyt *c* and the appearance of long-lived photoinduced absorption assigned to oxidized Zn porphyrin.[16, 17] The high charge separation yield observed for this zinc-substituted cytochrome was attributed to the longer singlet-excited-state lifetime of the Zn porphyrin ($\sim$3 ns) compared to that of the Fe-containing molecule. This longer lifetime favors efficient electron transfer from the singlet excited state into the TiO_2 electrode conduction band. This charge-separated state subsequently decayed as a result of interfacial charge recombination, with a half-time of 200 ms. We apply herein both methodologies, pulsed band-gap and direct excitation, to the study of interfacial electron transfer dynamics for cyt *b* maquette/TiO_2 films.

Pulsed laser excitation at 337 nm was employed to achieve TiO_2 band-gap excitation of Fe cyt *b* maquette/TiO_2. Transient absorption data were collected at probe wavelengths of 530 and 550 nm, which correspond to absorption maxima of the iron(III)

and iron(II) cyt *b* species, respectively. Transient data are shown as previously,[8] as the difference between the transient signals at 550 and 530 nm (Figure 7); in this way, contributions to the transient signal from photogenerated species within the TiO_2 electrode are removed. A long-lived positive signal is observed, assigned to photoreduction of the heme group from its iron(III)

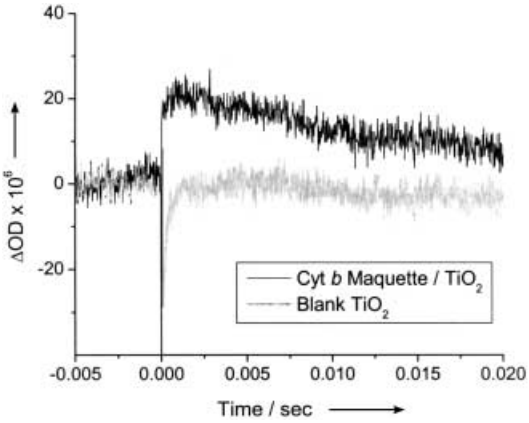

Figure 7. *Transient absorption data obtained following pulsed excitation of an iron(III) cyt* b *maquette/TiO_2 film at 337 nm. Control data are shown for a protein-free film. Data are shown as the difference between the transient optical signals at probe wavelengths of 560 and 530 nm; contributions to the transient signal from photogenerated species within the TiO_2 film are thus removed and only data resulting from redox changes of the iron(III) cyt* b *are shown.*

resting state to an iron(II) species. The rise time of this transient signal, which corresponds to the kinetics of heme reduction, is $\ll 100\,\mu s$. The transient signal decays with a half-time of approximately 20 ms, assigned to the return of the heme group to its iron(III) state. In contrast to the results of our previous studies of Fe cyt *c*/TiO_2 films,[8] prolonged UV illumination of the Fe cyt *b* maquette/TiO_2 film did not result in net heme reduction. This result is consistent with the more negative midpoint potential of the cyt *b* maquette.

Photoinduced electron transfer between the Zn cyt *b* maquette and TiO_2 electrode surface was achieved by employing pulsed laser excitation at 554 nm, an absorption maximum of the Zn cyt *b* maquette (see Figure 1). Transient absorption data were collected at a probe wavelength of 630 nm (Figure 8). Control data for a TiO_2 film in the absence of Zn cyt *b* showed no resolvable signal (Figure 8, gray line), which is consistent with the negligible optical density of the TiO_2 film alone at the excitation wavelength. For the Zn cyt *b* maquette/TiO_2 film, a rapid ($< 1\,\mu s$) absorption increase is observed that subsequently decays with a half-time of 7 ± 3 ms. The absorption increase is assigned to photoinduced absorption of the Zn protoporphyrin cation and photoinjected TiO_2 electron. The signal decay is assigned to charge recombination between these two species, consistent with our previous studies.[18] The absorption increase is of similar magnitude to that observed previously for Zn cyt *c*/TiO_2 films[16] and is indicative of a similarly high yield of charge separation and therefore an electron transfer rate

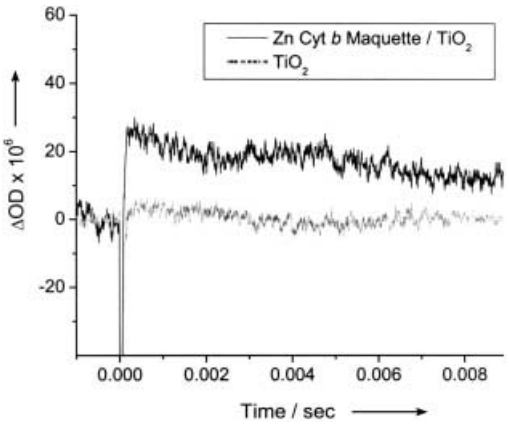

Figure 8. *Transient absorption data observed following pulsed laser excitation of a Zn cyt* b *maquette/TiO_2 film immersed in pH-7.0 buffer solution. Control data for a blank TiO_2 film are also shown. Data were collected at a probe wavelength of 630 nm with excitation at 554 nm.*

comparable with or faster than the Zn protoporphyrin excited state decay to the ground state, that is, a transfer rate of at least $10^8\ s^{-1}$.[19]

Discussion

We have demonstrated that immobilization upon nanocrystalline, mesoporous metal oxide substrates is a powerful route to investigating the function of a protein maquette. Strong adsorption of the cyt *b* maquette employed in this study on both TiO_2 and SnO_2 electrodes is observed, with a protein loading of up to 8 nmol cm^{-2} film. By analogy to our previous studies of natural protein adsorption,[8–10] this strong binding can be attributed to favorable electrostatic interactions between the negatively charged TiO_2 surface and the designed, positive patch of surface lysine residues localized around the heme binding pocket of the maquette, as illustrated in Figure 9. Spectroscopic, electrochemical, and ligand binding studies all confirm that the immobilized maquette maintains its solution structure and functionality. Essentially all ($> 90\,\%$) the immobilized protein was shown to be electrochemically active, which is consistent with a favorable orientation of the maquette on the film surface. Voltammograms of the films show quasireversible electron transfer from SnO_2 to the immobilized maquette, with the midpoint redox potential of the maquette similar to that observed on gold-modified electrodes and in solution.[4] The reversible electrochemistry we observed was obtained without the addition of any electron transfer mediators or promoters, which is in agreement with the suggested bound state of the maquette on the electrode and close proximity of the heme to the surface. The experiments were conducted under anaerobic conditions to avoid the surface reduction of oxygen, and at moderate potentials insufficient to generate molecular hydrogen, consistent with the absence of significant Faradaic currents in our experiments.

We employed two experimental techniques to probe interfacial electron transfer dynamics between the cyt *b* maquette and the TiO_2 electrode: cyclic voltammetry and transient

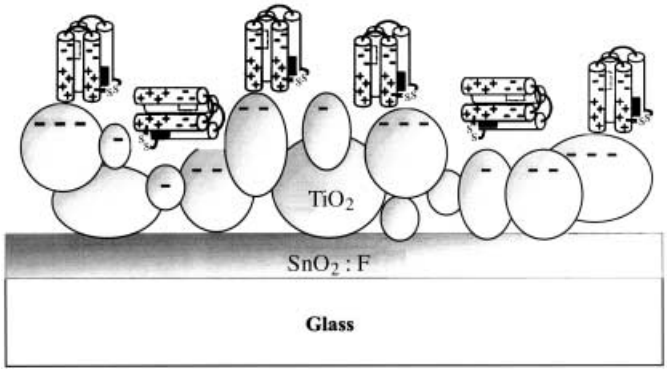

Figure 9. *Cytochrome* b *maquette structure: The 68 amino acid peptide is oxidized to form a disulfide bond and a four-helix bundle. The four-helix bandle can coordinate two heme groups by bis-histidyl ligation to form the heme protein maquette. The first heme group (black) binds tightly and the second heme group (dashed line) binds weakly. A ratio of 0.7 heme/bundle assured that the cyt* b *maquette did not contain more than one heme group. Glutamate residues (negatively charged aa) are distributed near the glycine loop, whereas lysine residues (positively charged aa) are concentrated at the opposite end of the protein. At neutral pH, binding of the cyt* b *maquette on the metal oxide film occurs by electrostatic interaction between the lysine residues of the cyt* b *maquette and the negatively charged oxygen moieties on the surface of the metal oxide electrode.*

absorption spectroscopy. The scan-rate dependence of the cyclic voltammetry reduction and reoxidation peaks allows determination of the zero free energy electron transfer rate constants. The reduction and reoxidation peaks exhibit distinct scan-rate dependencies indicative of electron transfer rate constants of around 1.4 and more than $100\,s^{-1}$ for the reduction and reoxidation processes, respectively. Such asymmetric behavior was not observed in cyclic voltammetry studies of the cyt *b* maquette adsorbed on modified gold electrodes,[4] nor was it observed in analogous studies of other natural proteins such as cyt *c* and hemoglobin absorbed on the same SnO_2 electrodes.[13] The observation of distinct rate constants for the reduction and oxidation processes can most easily be rationalized in terms of an electrostatically driven reorientation of the maquette on the electrode surface in response to the variation of the applied bias. Such reorientation processes have been discussed previously, for example for cyt *c* adsorbed on monolayer tin oxide electrodes.[19] The presence of such reorientation processes means that the rate constants reported herein can only be regarded as indicative of the electron transfer dynamics, rather than as unique rate constants.

Pulsed laser excitation of the Zn cyt *b* maquette adsorbed on TiO_2 electrodes produces a long-lived transient absorption signal. By analogy with our previous studies of Zn-substituted cyt *c*, this signal is assigned to the charge-separated state resulting from electron injection from the singlet excited state of the Zn cyt *b* into the TiO_2 conduction band. Consideration of the yield of this charge separation, as evidenced by the magnitude of the transient signal, indicates a rate constant for electron injection of comparable magnitude to the rate of singlet-excited-state decay to the ground state, $k_{inj} > 10^8\,s^{-1}$. The large magnitude of this rate constant compared to that obtained from the CV studies can largely be rationalized in terms of the large energetic driving force for this reaction. The singlet excited state oxidation potential of Zn cyt *b* is expected to be around 1 eV more negative than the TiO_2 conduction band edge, which allows essentially activationless electron injection into conduction band states with an energetic driving force ΔG equal to the reorganizational energy λ. In contrast, the CV measurements correspond to a zero free energy measurement of the electron transfer rate constant, with correspondingly large activation energy. According to nonadiabatic electron transfer theory, the ratio **P** of the rate constants for activationless and zero free energy electron transfer is given by Equation (1):

$$\mathbf{P} = \frac{k(\Delta G = \lambda)}{k(\Delta G = 0)} = \exp\left(\frac{\lambda}{4k_B T}\right) \quad (1)$$

If we assume a value of $\lambda \sim 1$ eV, as we have previously,[4] Equation (1) yields a value for the ratio **P** of 10^4. This analysis is clearly only approximate and neglects, for example, integration over the density of acceptor states, and differences in the TiO_2 and SnO_2 densities of states, but the method appears sufficient to explain the main origin of the difference between the rate constants observed in the CV and transient optical experiments.

After photoinduced charge separation, charge recombination between the oxidized Zn cyt *b* and electrons photoinjected into the TiO_2 electrode is observed with a half-time of 7 ms. This half-time is approximately one order of magnitude faster than we have reported for the analogous recombination reaction between Zn cyt *c* and TiO_2 electrodes. These faster recombination dynamics are consistent with those reported previously for both cyt *c* and cyt *b* maquettes adsorbed to modified gold electrodes.[4] These dynamics can be attributed to a stronger electronic coupling between the redox site and the metal oxide surface, which is consistent with the more exposed position of the heme group in the cyt *b* maquette compared to its position in cyt *c*.

For the Fe cyt *b* maquette/TiO_2 electrodes, photoinduced electron transfer can be initiated by band-gap excitation of the TiO_2 film at 337 nm. Such experiments avoid the need for Zn substitution of the heme group; however, the interpretation of data obtained from such band-gap excitation is complicated by the generation of a range of reactive species.[8] An appropriate subtraction procedure is therefore required to focus on redox changes of the adsorbed heme group. By using this approach, transient photoreduction of the iron(III) cyt *b* to iron(II) cyt *b* can be observed. The kinetics of both the photoreduction and the subsequent recombination reaction leading to reoxidation of the heme group are at least an order of magnitude faster than those we reported previously for Fe cyt *c*/TiO_2 electrodes. This result is again indicative of a stronger electronic coupling for the cyt *b* maquette/TiO_2 electrodes than for cyt *c*/TiO_2.

The immobilized cyt *b* maquette retains its ability to ligate carbon monoxide in its reduced iron(II) state, as demonstrated by the spectroelectrochemical data shown in Figure 6. These data exploit both the electrical conductivity of the film to achieve the electrochemical reduction of the immobilized cyt *b* to the desired iron(II) state, and the optical transparency and high protein loading of the film to allow the optical detection of spectral changes resulting from CO ligation. This albeit rather simple demonstration of functionality clearly demonstrates the

potential of this experimental approach. Our ability to synthesize protein maquettes with increasingly complex functionality is progressing rapidly. This progress will open up the potential to fabricate protein maquette/nanoporous electrode systems with functionality optimized for a wide range of technological applications.

Experimental Section

Chemicals and solvents: All chemicals were of reagent grade and all solutions were prepared in distilled deionized water. Horse heart cytochrome *c* (Type VI) and hemin were purchased from Sigma (Dorset, UK). Zn Protoporphyrin IX was purchased from Frontier Scientific (Lancashire, UK). All other chemicals were purchased from Merck (Dorset, UK). Sodium dihydrogen orthophosphate (0.01 M) was used to prepare the supporting electrolyte and its pH value was adjusted to 7 with NaOH. Fluorine-doped tin oxide coated (TEC 15) glass was purchased from Hartford Glass (Indiana, USA) and had a sheet resistance of 15 Ω^2.

Preparation of electrodes: Aqueous suspensions of anatase TiO_2 and SnO_2 nanoparticles were prepared as described elsewhere.[13, 20] Each suspension was applied to the surface of conducting glass slides and spread with a glass rod. Before suspension deposition, the conducting glass slides were washed with ethanol and heated at 450 °C. Masking the glass slides with Scotch tape controlled the thickness and the width of the suspension deposited. The slides were then allowed to dry in air before being heated for 20 min at 450 °C. The film thickness was measured with a step profilimeter at the end of the film preparation; typical film thicknesses were 4 or 8 μm. The resulting TiO_2 and SnO_2 films had nanocrystalline, mesoporous structures with a typical particle diameter of 18 nm and pore diameters of 15 – 20 nm. The slides were cut up to give film areas of 1 cm^2. Immediately prior to biomolecule immobilization, the films were reheated to 450 °C for 20 min and then allowed to cool to room temperature.

Peptide synthesis: The synthesis of the cyt *b* maquette apoprotein was conducted as reported previously.[4] The resulting 68 amino acid, 2-α-helix peptides (α_1-1-α_2) were dissolved in high-ionic-strength phosphate buffer (50 mM phosphate, 0.6 M NaCl) at pH 8.0 to yield a final concentration of 0.04 mM α_1-1-α_2. The peptide solution was then exposed to air to allow the cysteine residues to oxidize to form disulfide-linked homodimers (α_1-1-α_2-S-)$_2$. Heme-(α_1-1-α_2-S-)$_2$ formation was achieved by successive additions of 0.1 heme groups per binding site from a stock solution of iron(III) photoporphyrin IX (heme, 4 mM) in KOH (10 mM), until one heme group per bis-histidine site was present, as monitored by the appearance of the ligated heme Soret absorption maximum at 412 nm. The solution was well stirred during each addition and then allowed to equilibrate for 5 minutes. The final concentration of KOH in the aqueous solution was always lower than 1:1000 (v/v). The buffer composition was exchanged on a Sephadex G-25M column, which also served to remove unbound or only weakly bound heme groups. The same procedure was used for the incorporation of Zn protoporphyrin IX into the cyt *b* maquette apoprotein and led to a yield of more than 70% incorporation.

Protein immobilization: Protein immobilization was carried out by using methodologies we have previously employed for a range of natural proteins.[4–6] Immobilization was achieved by the immersion of 1-cm^2 TiO_2 or SnO_2 films in cyt *b* maquette solution (2 mL, 10 μM; 10 mM phosphate buffer, pH 7.0) at 4 °C for at least 3 – 4 days. Protein adsorption onto the TiO_2 or SnO_2 films was monitored by recording the UV/Vis absorption spectra of the immobilized films at room temperature on a Shimadzu UV-1601 spectrophotometer. Contributions to the spectra from scatter and absorption by the TiO_2 or SnO_2 film alone were subtracted; protein-free reference films were used as a measure of this background signal. Prior to all spectroscopic measurements, films were removed from the immobilization solution and rinsed in buffer solution to remove nonimmobilized protein.

Electrochemical measurements: Electrochemical and spectroelectrochemical experiments were performed on an Autolab PGStat 12 potentiostat. The spectroelectrochemical cell was a 3-mL, three-electrode cell with quartz windows. A platinum flag was used as the counter electrode, Ag/AgCl in 3 M KCl as the reference electrode, and the metal oxide film on conducting glass as the working electrode. The electrolyte, an aqueous solution of sodium phosphate (10 mM, pH 7.0), was thoroughly freed of air by bubbling with Argon prior to the experiments. For spectroelectrochemistry, the cell described above was incorporated into the sample compartment of the Shimadzu UV-1601 spectrophotometer and the absorption changes monitored as a function of applied potential. All potentials are reported with respect to Ag/AgCl. Carbon monoxide binding was monitored by absorption spectra collected before and after the addition of a saturated solution of CO. The saturated CO solution was prepared by bubbling CO gas through phosphate buffer solution (2 mL, 10 mM, pH 7.0) for 1 h at room temperature to give an approximate concentration of CO of 1 mM.[21]

Transient absorption spectroscopy: Transient absorption spectroscopy was employed to monitor the photoinduced interfacial electron transfer between the cyt *b* maquette and the TiO_2 films. Two approaches were used. The Fe cyt *b* maquette/TiO_2 films were excited at 337 nm (0.07 mJ cm^{-2}, 0.1 Hz), which corresponds to band-gap excitation of the TiO_2. The Zn cyt *b* maquette/TiO_2 film was excited at 554 nm (0.07 mJ cm^{-2}, 0.1 Hz), which corresponds to direct excitation of the Zn protoporphyrin. Data were collected at probe wavelengths in the range 530 – 630 nm. Details of the experimental apparatus have been given previously.[8] Probe light was provided by a 100-W tungsten lamp and wavelength selection was achieved by placing monochromators before and after the sample. Changes in optical density induced by the excitation pulses were monitored by an Si photodiode and custom-built amplification/filtering electronics, and digitized by a Tektronics TDS220 digital storage oscilloscope. Control data were collected by using films with no adsorbed protein. For all experiments, the film was covered in sodium phosphate solution (10 mM, pH 7.0).

Acknowledgements

Financial support from the Biotechnology and Biological Sciences Research Council, the Engineering and Physical Sciences Research Council, the National Institutes of Health (Grant nos. GM41048, F32 GM63388), and a Materials Research Science and Engineering Interdisciplinary Research Group grant from the National Science Foundation (Grant no. DMR0079909) is gratefully acknowledged. We also thank F. Duriaux, M. Grätzel, and E. Palomares for assistance in SnO_2 film preparation.

Keywords: cytochromes · electrochemistry · maquette · nanocrystals · transient spectroscopy

[1] D. E. Robertson, R. S. Farid, C. C. Moser, J. L. Urbauer, S. E. Mulholland, R. Pidikiti, J. D. Lear, A. J. Wand, W. F. DeGrado, P. L. Dutton, *Nature* **1994**, *368*, 425 – 432.
[2] J. W. Bryson, S. F. Betz, H. S. Lu, D. J. Suich, H. X. Zhou, K. T. O'Neil, W. F. DeGrado, *Science* **1995**, *270*, 935 – 941.
[3] M. L. Kennedy, B. R. Gibney, *Curr. Opin. Struct. Biol.* **2001**, *11*, 485 – 490, 12 – 13.
[4] X. Chen, B. M. Discher, D. L. Pilloud, B. R. Gibney, C. C. Moser, P. L. Dutton, *J. Phys. Chem. B* **2002**, *106*, 617 – 624.
[5] I. Willner, V. Heleg-Shabtai, E. Katz, H. K. Rau, W. Haehnel, *J. Am. Chem. Soc.* **1999**, *121*, 6455 – 6468.
[6] B. O'Regan, M. Grätzel, *Nature* **1991**, *353*, 737 – 740.
[7] R. Cinnsealach, G. Boschloo, S. Nagaraja Rao, D. Fitzmaurice, *Sol. Energy Mater. Sol. Cell.* **1999**, *57*, 107 – 125.
[8] E. Topoglidis, T. Lutz, R. L. Willis, C. J. Barnett, A. E. G. Cass, J. R. Durrant, *Faraday Discuss*. **2000**, *116*, 35 – 46.
[9] E. Topoglidis, C. J. Campbell, A. E. G. Cass, J. R. Durrant, *Langmuir* **2001**, *17*, 7899 – 7906.
[10] E. Topoglidis, A. E. G. Cass, B. O'Regan, J. R. Durrant, *J. Electroanal. Chem.* **2001**, *517*, 20 – 27.
[11] K. R. Meier, M. Grätzel, *Chem. Phys. Chem.* **2002**, 371 – 374.
[12] Q. Li, G. Luo, J. Feng, *Electroanalysis* **2001**, 13, 359 – 363.
[13] E. Topoglidis, Y. Astuti, F. Duriaux, M. Grätzel, J. R. Durrant, *Langmuir* **2003**, in press.
[14] E. Laviron, *J. Electroanal. Chem.* **1979**, *101*, 19 – 28.
[15] B. R. Gibney, F. Rabanal, K. S Reddy, P. L.Dutton, *Biochemistry* **1998**, *37*, 4635 – 4643.
[16] E. Topoglidis, C. J. Campbell, E. Palomares, J. R. Durrant, *Chem. Commun.* **2002**, *14*, 1518 – 1519.
[17] L. H. Guo, S. Mukamel, G. McLendon, *J. Am. Chem. Soc.* **1995**, *117*, 546 – 547.
[18] J. L. Willit, E. F. Bowden, *J. Electroanal. Chem.* **1987**, *221*, 265 – 274.
[19] We previously employed transient emission spectroscopy to demonstrate that charge separation for Zn cyt *c*/TiO_2 films proceeds directly from the Zn cyt *c* singlet excited state rather than following intersystem crossing to the triplet state.[16] We thus concluded that the rate constant for electron injection from the photogenerated Zn cyt *c* singlet excited state into the TiO_2 electrode was at least $10^8\ s^{-1}$.
[20] C. J. Barbe, F. Arendse, P. Comte, M. Jirousek, F. Lenzmann, V. Shklover, M. Grätzel, *J. Am. Ceram. Soc.* **1997**, *80*, 3157 – 3171.
[21] G. W. C. Kaye, T. H. Laby, *Tables of Physical and Chemical Constants*, 13th ed., Longmans, London, **1966**, p. 153.

Received: July 1, 2003 [F 707]

